

Differences between Ultrananocrystalline and Nanocrystalline Diamond Growth: Theoretical Investigation of C_xH_y Species at Diamond Step Edges

Maxie Eckert,* Erik Neyts, and Annemie Bogaerts

Research Group PLASMAN, Department of Chemistry, University of Antwerp,
Universiteitsplein 1, 2610 Antwerp, Belgium

Received June 16, 2010; Revised Manuscript Received July 20, 2010

ABSTRACT: The behavior of hydrocarbon species at step edges of diamond terraces is investigated by means of combined molecular dynamics–Metropolis Monte Carlo simulations. The results show that the formation of ballas-like diamond films (like UNCD) and well-faceted diamond films (like NCD) can be related to the gas phase concentrations of C_xH_y in a new manner: Species that have high concentrations above the growing UNCD films suppress the extension of step edges through defect formation. The species that are present above the growing NCD film, however, enhance the extension of diamond terraces, which is believed to result in well-faceted diamond films. Furthermore, it is shown that, during UNCD growth, C_xH_y species with $x \geq 2$ play an important role, in contrast to the currently adopted CVD diamond growth mechanism. Finally, the probabilities for the extension of the diamond (100) terrace are much higher than those for the diamond (111) terrace, which is in full agreement with the experimental observation that diamond (100) facets are more favored than diamond (111) facets during CVD diamond growth.

Introduction

The term *chemical vapor deposited (CVD) diamond* covers a broad range of synthetic diamond materials with a great variety of electrical and mechanical properties.^{1–4} *Nanocrystalline diamond (NCD)* refers to CVD diamond with crystallites less than 500 nm in size, whereas the term *ultrananocrystalline diamond (UNCD)* has been devised to describe CVD diamond with grains smaller than 10 nm.⁴ The differences between UNCD and NCD stem from the different growth conditions that are applied during microwave plasma-assisted CVD or hot filament CVD. NCD is grown by conventional diamond CVD conditions, i.e., from a hydrogen rich gas phase (typically 99% H_2 /1% CH_4).⁵ NCD consists of faceted diamond grains with diameters that are proportional to the film thickness, i.e., a small grain size polycrystalline diamond film that is not the ballas-like type grown with high CH_4 levels or under conditions that reduce the atomic hydrogen concentration in the gas phase.⁴ Instead, as the grain diameters are proportional to the film thickness, NCD becomes conventional microcrystalline diamond after a certain film thickness. Due to the hydrogen rich plasma that is applied for NCD growth, deposited sp^2 hybridized carbon atoms are etched back into the gas phase at a high rate,⁶ such that the sp^2 content in the film is rather low (< 5%). By reducing the hydrogen fraction in the plasma, etching of sp^2 hybridized carbon atoms is slowed down, which can lead to renucleation: A hydrogen-poor plasma (containing typically 97% Ar /2% H_2 /1% CH_4) results in UNCD film growth⁵ with a grain boundary content of around 10%.⁷ With decreasing grain size, the morphology of the films gradually changes from faceted diamond crystallites into ballas-like (ball-like) diamond.^{8,9}

Up to the present, the different growth regimes and resulting morphologies of UNCD and NCD are mainly related to

the differences between the gas phase compositions, i.e., the amount of atomic hydrogen that is present above the surface of the growing film. Atomic hydrogen is known to etch graphite phases much faster than diamond phases,¹⁰ such that a hydrogen rich plasma (as applied for NCD growth) prevents the accumulation of sp^2 hybridized phases within the growing film.

In the present paper, it is investigated whether the presence or absence of another important mechanism for crystal growth may explain the differences between the ballas-like (UNCD) and well-faceted (NCD) growth. The growth of well-faceted NCD films is associated with the so-called “step-flow growth mechanism” of diamond.¹¹ This mechanism, which is thought to explain the growth of smooth diamond surfaces,^{12,13} can be summarized as follows:^{13–16} First, a hydrocarbon species from the gas phase sticks to a carbon atom on a diamond terrace, that is, at a flat diamond surface. After chemisorption to the diamond surface, the hydrocarbon species can migrate over the terrace until it meets the boundary of that terrace, i.e., the so-called step edge. When reaching a step edge, the hydrocarbon species incorporates into the lattice by forming a C–C bond to an atom that belongs to a lower-lying terrace; that is, the diamond terraces grow by extension at their steps. Although the step-flow growth mechanism is widely accepted,^{11–13} the effect of migrating hydrocarbon species at diamond surfaces is still controversial.¹⁴ Alternatively, growth via step edges can be explained by “preferential etching”:¹⁷ Hydrocarbon species at flat diamond surfaces are etched away faster than when adsorbed next to a step edge, such that hydrocarbon species will preferentially reside at step edges. When stuck to a step edge, the hydrocarbon species can pursue the diamond lattice by extending the terrace.

In a recent publication, May et al. point out that a better insight into the behavior of species at diamond step edges would help to predict the onset of the UNCD and NCD morphologies.¹⁴ Previously, classical MD,¹⁸ first-principles density-functional theory,^{11,19} and first-principles density-functional

*To whom correspondence should be addressed. Telephone: +32 32 65 23 82. Fax: +32 32 65 23 76. E-mail: maxie.eckert@ua.ac.be. Web: <http://www.ua.ac.be/plasma>.

MD²⁰ simulations have been applied for the investigation of adsorption (i.e., the short-term behavior) of hydrocarbon species at or close to diamond step edges. However, when simulating crystal growth, longer time scale processes need to be considered as well. Until now, the longer time scale behavior of hydrocarbon species at step edges has not been investigated. For instance, it is not clear if hydrocarbon groups migrate off the step edge and, if yes, if they initiate lattice defects by preferentially forming C–C bonds that distort the diamond structure or if they migrate down the step edge without the formation of new C–C bonds between the step edge and the lower-lying terrace (migration from the upper-lying to the lower-lying terrace).

Migration of hydrocarbon species at flat diamond 100(2 × 1) and (111)1 × 1 surfaces has been studied at different levels of theory,^{15,16,21–23} whereas migration down a step edge has received less attention. Recently, Richley et al. attempted to describe the possible routes for a CH₂ species migrating down step edges of diamond (100)2 × 1 and (111)1 × 1 terraces.²⁴ In the present paper, for various species, the relation is examined between their longer time scale behavior at diamond step edges and the resulting film morphology. That is, we investigate which C_xH_y species enhance the step-flow mechanism and which C_xH_y species suppress that mechanism. If the step-flow mechanism is enhanced by species with a high concentration above the growing film, the morphology will be expected to be faceted (like NCD); if this mechanism is suppressed, a ballas-like morphology (like UNCD) will be more probable.

The different gas-phase chemistry and concentration profiles of various C_xH_y species for both UNCD and NCD growth conditions have been studied in detail.^{5,25} Calculations of gas phase concentrations⁵ and molecular dynamics (MD) investigations of the reaction behavior of various hydrocarbon species at diamond surfaces²⁶ demonstrate that C, C₂H₂, C₃, and C₄H₂ are the most important growth species for UNCD growth within their C_xH_y series ($x = 1–4$).^{5,26} For NCD, the more hydrogen rich species CH₃, C₂H₂, C₃H₂, and C₄H₂ appear to be the most important growth species.

Classical MD simulations are a very powerful tool for the simulation of crystal growth, since the dynamics of the system (including chemisorption and desorption of atoms) are taken into account.²⁷ Nevertheless, at maximum, the range of MD simulations reaches the time scale of nanoseconds. Hence, relaxation processes and diffusive events, which take place at the microsecond time scale,²⁸ cannot be simulated by means of MD. Therefore, we coupled our MD model to the Metropolis Monte Carlo (MMC) algorithm, such that combined MD-MMC simulations can be carried out.^{29,30} The MD part of the code answers for the simulation of particle impacts, whereas the MMC part simulates the further evolution of adatoms at the growing surface. The MMC algorithm was developed in its original form in the 1950s.³¹ Its most important feature is that no transition mechanisms need to be known or assumed in order to simulate the longer time scale behavior of a system. Indeed, for other Monte Carlo methods that were developed for the simulation of crystal growth, e.g. the kinetic Monte Carlo method, a catalogue of transition mechanisms has to be composed.^{32,33} Unfortunately, the completeness of this catalogue, and therefore the reliability of the simulations, depends on the intuition of the scientist designing the catalogue. We showed that when coupling the MMC method to an MD code, the integral evolution of impacting species during thin film growth can be followed.^{29,30} This was also found by others.³⁴ In ref 29, we have shown that the calculation time of

the MMC simulations was typically 1 order of magnitude shorter than the calculation time of the longer time scale MD simulations that were carried out for the verification of the MMC simulations.²⁹ In a previous study, we examined the behavior of hydrocarbon species at mono- and biradical sites when stuck at flat diamond (100) and (111) surfaces.³⁰ It was concluded that, in contrast to the general assumption, C_xH_y species with $x \geq 2$ might play an important role during the nucleation of new diamond layers.³⁰ In a recent paper, May et al. also suggest that other hydrocarbons than the C₁H_y species might affect the growth rate of (U)NCD.¹⁴ For that very reason, more insight is requested into the role of various hydrocarbon species, including C_xH_y species with $x > 1$. In this paper, we present the results of a combined MD-MMC study that intends unraveling the routes for hydrocarbon species stuck to step edges.

Models and Methods

Construction of Step Edges. Different types of step edges for both the diamond (100) and (111) terraces are possible. It needs to be decided (i) which step height is simulated (e.g., single-layer or bilayer step edges) and (ii) which geometry the vertical edges are composed of, i.e., which crystal planes are juxtaposed between the upper- and lower-lying terraces.

The current understanding of the step-flow growth mechanism implies that diamond terraces are monatomic layers that are pursued by the formation of bonds between a hydrocarbon species at the step edge and the lower-lying diamond terrace.³⁵ Nevertheless, besides single-layer step edges, bilayer (and higher) step edges have also been observed experimentally.³⁶ This might be explained by the fact that, depending on the geometry of the step edges, two terraces proceeding in the same direction do not grow at the same rates.^{12,35} As a certain terrace catches up with its lower-lying terrace, a bilayer step edge might be formed. As the proceeding of diamond terraces is assumed to occur initially at the monatomic height steps,^{12,37,35,38} only single-layer step edges are simulated in the present investigation.

For both diamond (100) and (111) terraces, there are two different single-layer step edges that can delimit the terraces; see Figures 1 and 2. For diamond (100), the dimerization direction on the upper terrace is either perpendicular or parallel to the step edge (see Figure 1a and b, employing Chadi's convention, indicated by "S_A" and "S_B", respectively³⁹). By means of scanning tunneling microscopy experiments, Kawarada et al. have shown that growth occurs preferentially at the S_B steps.³⁷ Therefore, we chose to simulate diamond (100) terraces that have boundaries of type S_B.

For diamond (111), the vertical plane can either be the (100) plane or the (111) plane (see Figure 2a and b, "type A" and "type B", respectively¹¹). Larsson has shown that the adsorption of hydrocarbon species at biradical sites (see below) is energetically more favorable for type B;¹¹ therefore, this geometry will be simulated.

The probability of two surface sites chosen at random both being radicals; that is, they form a biradical site, is as low as 0.01.⁴⁰ Nevertheless, as in previous investigations by others,^{18,23,24} it is assumed here that radicals stuck to a step edge with an adjacent radical site might affect the growth of diamond to a great extent. This assumption is supported by Monte Carlo calculations that draw attention to the importance of biradical sites for the growth of CVD diamond.^{14,41}

Due to sterical effects at the step edges of diamond (111) terraces, the adsorption of hydrocarbon species on the vertical edge is energetically more favorable than that at the lower terrace.¹¹ Therefore, at the biradical site, the chosen adsorption site for the investigated hydrocarbon species is the vertical edge (see Figure 2c). Due to lack of data of the adsorption energy for different sites at the diamond (100) S_B step edge, we assume that the same sterical effects as for the case of diamond (111) will favor adsorption at the vertical step edge; see Figure 1c.

The structures that will be impacted by the species relevant for UNCD and NCD growth have temperatures of 800 and 1100 K,

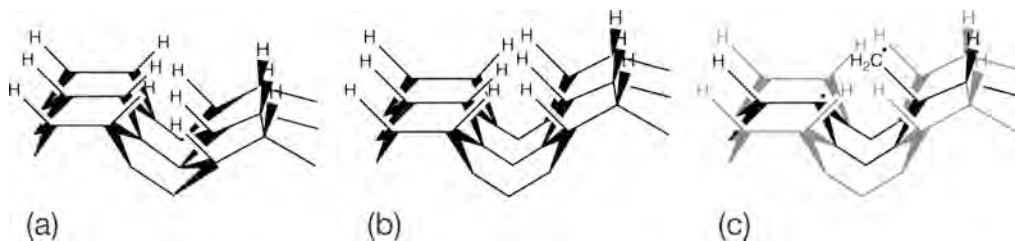


Figure 1. Diamond (100) step edges. Hydrogenated “S_A” step edge (a) and “S_B” step edge (b).³⁹ In the present simulations, adsorbed hydrocarbon species, e.g. CH₂, at S_B step edges are investigated as indicated in part c; at the lower terrace, a surface radical (“dangling bond”) is available (see text). For reasons of clarity, in part c, the middle atoms and bonds are colored black and the others gray, which is also done for the graphics in the Results section.

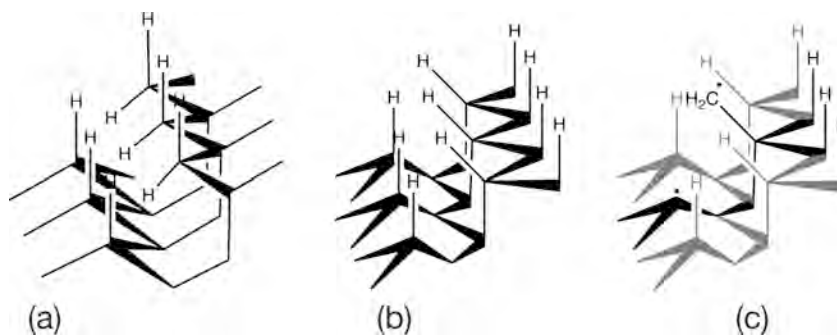


Figure 2. Diamond (111) step edges. Hydrogenated “type A” step edge (a) and “type B” step edge (b).¹¹ In the present simulations, adsorbed hydrocarbon species, e.g. CH₂, at type B step edges are investigated as indicated in part c; at the lower terrace, a dangling bond is available (see text). For reasons of clarity, in part c, the middle atoms and bonds are colored black and the others gray, which is also done for the graphics in the Results section.

respectively. Indeed, UNCD can be grown at substrate temperatures as low as 800 K, whereas NCD is grown at 1100 K.⁴ Therefore, the simulation conditions for the UNCD and NCD species at the step edges differ by the system temperature. The UNCD species (see below) are investigated at a substrate temperature of 800 K, and the NCD species (see below) at a substrate temperature of 1100 K. For each of the two temperatures, two step edges have been constructed: The step edge of a diamond (100)2 × 1 terrace (see Figure 1c) and the step edge of a diamond (111)1 × 1 terrace (see Figure 2c). In this way, four different input configurations for the MD simulations can be distinguished. Before the impacts, the partially hydrogenated diamond substrates contain 468 (diamond (100)2 × 1 terrace) and 448 (diamond (111)1 × 1 terrace) carbon atoms. The structures hold additionally 50 and 70 H atoms, respectively. To prevent translation of the cell due to momentum transfer of impacting species, the lower two atomic layers (100 and 128 carbon atoms for diamond (100) and (111), respectively) are kept fixed. In the ±x- and ±y-direction (parallel to the terraces), periodic boundary conditions are applied.

Selection of the C_xH_y Species. For the selection of hydrocarbon species that will be investigated, the absolute number of sticking events during the growth of UNCD and NCD is predicted. As an approximation for the sticking coefficients of the C_xH_y species at diamond step edges, we use values for flat diamond (100) and (111) surfaces.²⁶ Furthermore, May et al. presented the concentrations of those species in ref 5. For UNCD, the product of concentration and sticking coefficient is the highest for C₂H₂ and C₃ (~10¹⁴ cm⁻³), followed by C₃H₂, C₄H₂ (~10¹³ cm⁻³), C₂H, and C (~10¹² cm⁻³). For NCD, the product of concentration and sticking coefficient is the highest for C₂H₂ (~10¹³ cm⁻³), followed by CH₃ and C₃H₂ (~10¹² cm⁻³). These species are investigated in the present study. In addition, as CH₂ (through hydrogen abstraction of CH₃) is thought to play an important role during diamond growth,⁴² CH₂ completes the list of hydrocarbon species of interest. However, CH₂ is the only investigated species originating from hydrocarbon abstraction of another species, in order to keep the list of investigated hydrocarbon species reasonable.

Simulation Model. In this section, the MD-MMC simulation model is explained very briefly. All details of the MD-MMC model can be found in refs 29 and 30. The term MD-MMC simulation

refers to simulations in which MD and MMC methods are alternated. During one MD-MMC cycle, a hydrocarbon species impacts a diamond structure, which is described by means of MD; the further evolution at the surface is simulated by the MMC method. In Monte Carlo simulations, the system evolves stochastically (i.e., based on random numbers), whereas MD simulations are deterministic. In MD simulations, the atoms of the considered system move based on Newtonian dynamics. During the simulation, the positions and velocities of the atoms are calculated for each discrete time step by integrating the equations of motion. In the MD model, the interaction between the atoms is described by a potential function.⁴³ Here, we apply the well-known Brenner potential, an empirical potential function for hydrocarbon structures.⁴⁴ In contrast to other potential functions, this function describes well the structure of diamond surfaces and the energetics of the reconstruction, in agreement with quantum mechanical calculations.²⁷

In MMC simulations, the system evolves entirely based on its thermodynamic properties; that is, no activation barriers are taken into account. One MMC simulation consists of a number of MMC cycles. In each MMC cycle, one *trial move* is carried out: An atom or a cluster of atoms is translated or rotated (the latter only applies to clusters). Depending on the energy difference caused by the random move, the trial move is accepted or rejected. If the potential energy remains constant or decreases, the move is accepted. Otherwise, the probability that the move will be accepted is derived from Boltzmann's occupation probabilities for the states of a canonical ensemble;³¹ see below.

The validation of the MD-MMC model was accomplished by comparing resulting configurations from the combined MD-MMC simulations with longer time scale MD simulations²⁹ as well as by the investigation of the insertion mechanism of CH₂ species into a dimer at the diamond (100)2 × 1 surface.³⁰

MD Part of the Model. First, the impacts of the hydrocarbon species on diamond step edges are simulated by means of MD. All simulations are carried out for the two step edges, i.e., the step edge at diamond (100)2 × 1 as well as the step edge at diamond (111)1 × 1. Note that besides the different gas phase mixtures that are applied for the deposition of UNCD and NCD (see above), different substrate temperatures are applicable. Before the simulation of

impacts, the substrate was thermalized by the Berendsen heat bath at 800 and 1100 K, respectively (a very detailed description of the thermalization can be found in ref 26). However, during the MD part of the MD-MMC simulation, no further heat bath is applied; that is, the system evolves freely.

In order to maximize the sticking probability, all simulated impacts are normal to the terraces⁴⁵ and close to the dangling bond at the vertical plane of the edge; that is, the initial position of the impacting species in the $\{x,y\}$ -surface is randomly chosen within 1 \AA^2 of the dangling bond. The impacting species are initially placed at a distance greater than the outer cutoff radius, thus at a z -value for which the interaction energy between the surface and the species can be neglected. As an estimation of the species' translational, rotational, and vibrational energies, we assume a gas temperature of 2120 K (as calculated for UNCD deposition⁵). All impacts are followed for 2.0 ps. Once the MD integration time of 2.0 ps is reached, the output configuration is subject to the starting MMC simulation.

MMC Part of the Model. As soon as the MD simulation is finished, the MMC part of the simulation is started. For each species at each of the two step edges, 50 MMC simulations were carried out to have some statistically justified outcome.

The MMC simulation starts with listing the atoms that will be allowed to undergo trial moves in the MMC simulation. The number of atoms that are explicitly considered in the simulation of relaxation processes is restricted to the atoms that do not belong to the crystalline phase,²⁹ i.e., the *adatoms*. For this investigation, the atoms that have impacted the input structures during the MD simulation, i.e., the atoms that are part of the investigated species, are classified as adatoms. In order not to push the system into a crystalline configuration, the list of adatoms is not modified during one MMC simulation. However, the list of the adatoms is only the first part of the list of *movers*. In analogy to other MC approaches,^{46–48} the local environment of the adatoms is taken into account: The neighbors of the adatoms are also allowed to be displaced. Furthermore, in the list of movers, the adatoms are stored both individually and as clusters (defined as adatoms connected by chemical bonds). The clusters are stored *twice* in the list of movers, accounting for both translation and rotation of the cluster. In order to take the changes due to the trial moves into account, the neighbors and clusters of adatoms are re-evaluated after every accepted move.

During each MMC cycle, one member of the movers list is chosen randomly. If the mover is an atom, a randomly chosen (x,y,z) -displacement will be determined. For each dimension i , the translation is calculated as follows:^{29,31} $\delta_{\max,i}(2rand_i - 1.0)$, where $\delta_{\max,i}$ represents the maximum displacement in the considered direction and $rand_i$ is a random number $\in [0,1]$. The values of $\delta_{\max,x}$ and $\delta_{\max,y}$ are equal to 2.8 Å for both the diamond (100) and (111) surfaces, whereas the value of $\delta_{\max,z}$ equals 0.6 Å and 0.8 Å for diamond (100) and (111), respectively.

When a cluster is chosen from the movers list, it has to be decided whether the chosen cluster will be rotated or translated (with each a probability of 50%). A trial translation of the cluster is carried out as explained above; that is, all adatoms that are part of the cluster are displaced by the same random translation. However, if the trial move is a rotation, the cluster is rotated by a random rotation angle about an arbitrary axis. This axis is constructed through the crystalline atom to which the cluster is bound, i.e., a crystalline atom.³⁰

When the trial configuration is determined, the potential energy difference $\Delta E_{m \rightarrow n}$ between the original configuration m and the trial configuration n is calculated: $\Delta E_{m \rightarrow n} = E_n - E_m$. The trial configuration is accepted, if the energy decreases due to the trial move or remains constant. If the energy increases, the transition probability has to be calculated. This probability is derived from the Boltzmann distribution function for the occupation probability P_i for a state i of a canonical ensemble at temperature T ,⁴⁹

$$P_i = \frac{1}{Z} e^{-E_i/k_B T}, \text{ with the partition function} \quad (1)$$

$$Z = \sum_j e^{-E_j/k_B T}$$

E_i represents the energy of state i , k_B represents the Boltzmann constant, and j runs over all states of the canonical ensemble. The

probability of the transition from state m to a higher energy state n , $P_{m \rightarrow n}$, is now calculated by the ratio of the occupation probabilities P_m and P_n :³¹

$$P_{m \rightarrow n} = e^{-\Delta E_{m \rightarrow n}/k_B T} \quad (2)$$

It is now decided by a random number $rand_j \in [0,1]$ whether the transition to the higher energy state is accepted or not: For $rand_j > P_{m \rightarrow n}$, the trial move is rejected. Otherwise, it is accepted.

After 10^4 – 10^5 MMC cycles, the number of adjacent rejected moves equals half the number of all trial moves that have been carried out, and the simulation is forced to stop.²⁹

Results and Discussion

After the MD simulation of the impacting hydrocarbon species, all stuck hydrocarbons have one bond with the surface (as shown in Figures 1c and 2c). At flat diamond surfaces, this is the most probable configuration for substrate temperatures between 800 and 1100 K.²⁶ However, Perry et al. find by means of classical MD simulations that, for impacting C_2H_2 species on diamond (111) type B step edges at a system temperature of 1250 K, the probability is quite high that a second C–C bond is formed to the dangling bond at the lower-lying terrace.¹⁸ The lower temperatures that are applied in our simulations might explain why we do not observe the formation of a second C–C bond *within the MD integration time*, but only when applying the MMC simulations, as shown below.

In Tables 1–4, the resulting configurations together with the corresponding probabilities from the MMC simulations are presented. Here, it needs to be noted that the formation of new carbon 6-rings pursues the diamond structure, thereby extending the upper terrace. At the diamond (100) step edge, the bond formation between the dangling bond at the lower-lying terrace and the first carbon adatom bonded to the step edge results in a carbon 6-ring. At the diamond (111) step edge, however, two carbon adatoms have to bridge the step edge and the dangling bond at the lower lying diamond terrace, in order to pursue the diamond structure. The formation of other C–C bonds that bridge the upper- and lower-lying terrace results in nondiamond bonds, i.e., defects at the step edges.

In the following, the resulting configurations from the MMC simulations are discussed first for the species important for UNCD growth, followed by the discussion of the results for the species important for NCD growth. Furthermore, we expound the implications for the growth of UNCD and NCD.

C_xH_y Species Important for UNCD Growth. In Tables 1 and 2, the resulting structures for the species important for UNCD growth are presented for the diamond (100) and (111) terraces, respectively, accompanied by the corresponding probabilities.

From Table 1, it can be seen that all investigated species important for UNCD growth are capable of pursuing the upper terrace at the diamond (100) step edge (i.e., the probability of 6-ring formation is greater than 0.00 for all cases). The species that are the most probable of extending the diamond (100) terrace (with a probability higher than 0.7) are C and C_2H . The other species form new carbon 6-rings with a probability between 0.2 and 0.4, except for C_3H_2 (which has a probability of only 0.02 to pursue the diamond lattice). As the probability of 6-ring formation decreases (down the table), the probability that other C–C bonds are formed (i.e., defect formation) increases: As is clear from the third column of Table 1, C_3H_2 has the highest probability of defect formation (0.96). The configurations presented in the third column contain bridging C–C bonds

Table 1. Reaction Mechanisms of C_xH_y Species Important for UNCD Growth Occurring at Step Edges Delimiting Diamond (100) Terraces^a

input configuration	resulting configuration			
	new carbon 6-rings	other	migration	no new bonds
C				
Probability	0.96 (0.84)	0.02 (0.02)	0.00	0.02
ΔE (eV) =	-1.89 (-1.65)	-0.58 (-0.58)		0.00
C ₂ H				
Probability	0.74 (0.74)	0.20 (0.20)	0.02 (0.02)	0.04
ΔE (eV) =	-0.28 (-0.28)	-0.94 (-0.94)	+0.29 (+0.29)	0.00
C ₄ H ₂				
Probability	0.40 (0.16)	0.58 (0.30)	0.00	0.02
ΔE (eV) =	-7.46 (-7.25)	-7.50 (-7.87)		0.00
C ₂ H ₂				
Probability	0.32 (0.20)	0.50 (0.30)	0.16 (0.16)	0.02
ΔE (eV) =	-5.86 (-4.33)	-7.05 (-6.67)	-7.63 (-7.63)	0.00
C ₃				
Probability	0.28 (0.26)	0.70 (0.36)	0.00	0.02
ΔE (eV) =	-6.33 (-6.34)	-5.81 (-5.54)		0.00
C ₃ H ₂				
Probability	0.02 (0.02)	0.96 (0.72)	0.00	0.02
ΔE (eV) =	-6.50 (-6.50)	-5.78 (-5.99)		0.00

^a In the left column, the input configuration is shown. In the other columns, the resulting configurations calculated from 50 MMC simulations are shown: In the second column, the configuration of the carbon 6-ring, which is the essential step in the diamond growth, is shown, together with its relative occurrence (*Probability*) and energy decrease (ΔE) due to the configuration change. The energy decrease is calculated as the average energy decrease for the resulting configurations with the same C–C bonding structure, with respect to the energy configurations that do not exhibit bond changes after the MMC simulation. For completeness, the numbers within the parentheses correspond to the values that apply to the displayed structures (with its specific C–H bonding structure). In the third column, the most probable of the other resulting configurations with changed C–C bonds is displayed, together with the probability of C–C bond changes different from the formation of carbon 6-rings. In the fourth column, the configuration after migration onto the lower-lying terrace is shown (if observed), together with its formation probability and energy difference. The probability that no new bonds are broken or formed is given in the rightmost column. The species are sorted from top to bottom of the table by decreasing probability of carbon 6-ring formation.

between the upper- and lower-lying terrace, all resulting in carbon 7-rings, except for C (which forms a bond with a neighboring carbon atom at the step edge) and C₂H₂ (which abandons one H atom to the dangling bond; that is, the resulting structure consists of C₂H and the passivated

dangling bond at the lower-lying terrace). C₂H is thus the only species that does not contribute to defect formation at the step edge.












In the fourth column of the table, the probability of migration to the lower terrace is presented. Note that the

Table 2. Reaction Mechanisms of C_xH_y Species Important for UNCD Growth Occurring at Step Edges Delimiting Diamond (111) Terraces^a

input configuration	resulting configuration			
	new carbon 6-rings	other	migration	no new bonds
C_2H 				
Probability	0.34 (0.18)	0.02 (0.02)	0.26 (0.26)	0.38
ΔE (eV) =	-2.06 (-2.38)	-0.41 (-0.41)	-0.42 (-0.42)	0.00
C_3H_2 				
Probability	0.30 (0.16)	0.46 (0.18)	0.00	0.24
ΔE (eV) =	-4.28 (-3.95)	-1.62 (-0.01)		0.00
C_2H_2 				
Probability	0.14 (0.14)	0.10 (0.04)	0.00	0.76
ΔE (eV) =	-5.15 (-5.15)	-0.56 (+0.56)		0.00
C_4H_2 				
Probability	0.12 (0.04)	0.76 (0.40)	0.00	0.12
ΔE (eV) =	-3.18 (-3.07)	-1.89 (-1.83)		0.00
C_3 				
Probability	0.04 (0.02)	0.88 (0.80)	0.06 (0.06)	0.02
ΔE (eV) =	-3.56 (-2.24)	-2.79 (-2.65)	-2.36 (-2.36)	0.00
C 				
Probability	0.00	0.94 (0.54)	0.04 (0.04)	0.02
ΔE (eV) =		-4.04 (-4.53)	-3.43 (-3.43)	0.00

^a In the left column, the input configuration is shown. In the other columns, the resulting configurations calculated from 50 MMC simulations are shown: In the second column, the configuration of the carbon 6-ring, which is the essential step in the diamond growth, is shown, together with its relative occurrence (*Probability*) and energy decrease (ΔE) due to the configuration change. The energy decrease is calculated as the average energy decrease for the resulting configurations with the same C–C bonding structure, with respect to the energy configurations that do not exhibit bond changes after the MMC simulation. For completeness, the numbers within the brackets correspond to the values that apply to the displayed structures (with its specific C–H bonding structure). In the third column, the most probable of the other resulting configurations with changed C–C bonds is displayed, together with the probability of C–C bond changes different from the formation of carbon 6-rings. In the fourth column, the configuration after migration onto the lower-lying terrace is shown (if observed), together with its formation probability and energy difference. The probability that no new bonds are broken or formed is given in the rightmost column. The species are sorted from top to bottom of the table by decreasing probability of carbon 6-ring formation.

Table 3. Reaction Mechanisms of C_xH_y Species Important for NCD Growth Occurring at Step Edges Delimiting Diamond (100) Terraces^a

input configuration	resulting configuration			
	new carbon 6-rings	other	migration	no new bonds
CH_2 				
Probability	0.86 (0.86)	0.06 (0.04)	0.06 (0.06)	0.02
ΔE (eV) =	-2.49 (-2.49)	+0.08 (+0.08)	-0.43 (-0.43)	0.00
C_2H_2 				
Probability	0.46 (0.36)	0.52 (0.26)	0.00	0.02
ΔE (eV) =	-5.86 (-4.33)	-7.05 (-6.67)		0.00
CH_3 				
Probability	0.00	0.98 (0.98)	0.00	0.02
ΔE (eV) =		-4.16 (-4.16)		0.00
C_3H_2 				
Probability	0.00	0.98 (0.76)	0.00	0.02
ΔE (eV) =		-5.80 (-5.99)		0.00

^aIn the left column, the input configuration is shown. In the other columns, the resulting configurations calculated from 50 MMC simulations are shown: In the second column, the configuration of the carbon 6-ring, which is the essential step in the diamond growth, is shown, together with its relative occurrence (*Probability*) and energy decrease (ΔE) due to the configuration change. The energy decrease is calculated as the average energy decrease for the resulting configurations with the same C–C bonding structure, with respect to the energy configurations that do not exhibit bond changes after the MMC simulation. For completeness, the numbers within the brackets correspond to the values that apply to the displayed structures (with its specific C–H bonding structure). In the third column, the most probable of the other resulting configurations with changed C–C bonds is displayed, together with the probability of C–C bond changes different from the formation of carbon 6-rings. In the fourth column, the configuration after migration onto the lower-lying terrace is shown (if observed), together with its formation probability and energy difference. The probability that no new bonds are broken or formed is given in the rightmost column. The species are sorted from top to bottom of the table by decreasing probability of carbon 6-ring formation.

term *migration* refers only to configurations that include a bond of the species under study to the lower lying terrace, and no longer a bond to the upper lying terrace. Other configurations, including bridging configurations that exhibit bonding of the species to the lower lying terrace as well as to the upper lying terrace, are held within the other columns. The migration mechanism is observed only for C_2H and C_2H_2 with a low probability (0.02 and 0.16, respectively; see Table 1).










At the diamond (100) step edge, the probability is very low that the bonding connectivity does not change under the influence of the MMC simulation (≤ 0.04 ; see the rightmost column of Table 1). This implies that the investigated species all have a high probability to undergo relaxation events.

As was discussed in ref 30, we see here that as the probability of 6-ring formation decreases (downward the tables), no clear trend regarding the energetics can be observed: The energetics of the formation of carbon 6-rings and other structures do not imply which resulting structure is favored. This implies that it is not the minimum energy configuration that determines the resulting structure but the configuration

space during the MMC simulation. We therefore encourage calculations at a higher level of theory that are not confined to thermodynamical data of adsorbed C_xH_y species but include kinetic information as well.

In Table 2, the results for the species important for UNCD growth at the diamond (111) step edges are presented. We can see that the species do not pursue the diamond lattice at the diamond (111) step edge to the same extent as at the diamond (100) step edge: The species that are the most capable of extending the diamond (111) terrace are C_2H and C_3H_2 , with a probability of 6-ring formation of only 0.34 and 0.30, respectively. The other species contribute to the extension of the (111) terrace with a probability of less than 0.2. Furthermore, when comparing to the (100) step edge, it is much more probable that no bonds are broken or new bonds are formed, as appears from the last column (see Table 2): for example, C_2H_2 has a probability of 0.76 to stay in the configuration that was obtained by the MD simulation. The difference of the reactivity at the diamond (100) and (111) terraces provides an atomic scale explanation for the different growth rates of the terraces (as will be discussed below).

Table 4. Reaction Mechanisms of C_xH_y Species Important for NCD Growth Occurring at Step Edges Delimiting Diamond (111) Terraces^a

input configuration	resulting configuration			
	new carbon 6-rings	other	migration	no new bonds
C_3H_2 				
Probability	0.34 (0.18)	0.38 (0.12)	0.00	0.28
ΔE (eV) =	-4.28 (-3.95)	-1.82 (-0.01)		0.00
C_2H_2 				
Probability	0.14 (0.14)	0.24 (0.20)	0.00	0.62
ΔE (eV) =	-5.15 (-5.15)	+0.25 (+0.56)		0.00
CH_2 				
Probability	0.00	0.02 (0.02)	0.00	0.98
ΔE (eV) =		-0.09 (-0.09)		0.00
CH_3 				
Probability	0.00	0.00	0.00	1.00
ΔE (eV) =				0.00

^aIn the left column, the input configuration is shown. In the other columns, the resulting configurations calculated from 50 MMC simulations are shown: In the second column, the configuration of the carbon 6-ring, which is the essential step in the diamond growth, is shown, together with its relative occurrence (*Probability*) and energy decrease (ΔE) due to the configuration change. The energy decrease is calculated as the average energy decrease for the resulting configurations with the same C–C bonding structure, with respect to the energy configurations that do not exhibit bond changes after the MMC simulation. For completeness, the numbers within the brackets correspond to the values that apply to the displayed structures (with its specific C–H bonding structure). In the third column, the most probable of the other resulting configurations with changed C–C bonds is displayed, together with the probability of C–C bond changes different from the formation of carbon 6-rings. In the fourth column, the configuration after migration onto the lower-lying terrace is shown (if observed), together with its formation probability and energy difference. The probability that no new bonds are broken or formed is given in the rightmost column. The species are sorted from top to bottom of the table by decreasing probability of carbon 6-ring formation.

Perry et al. have simulated impacts of hydrocarbon species, including C_2H , on the diamond (111) type B step edge by means of classical MD.¹⁸ For a system temperature of 1250 K and a MD integration time of less than 1.0 ps, they find that only 3% of the adsorbed species form a carbon 6-ring by bridging the step edge and dangling bond at the lower-lying terrace.¹⁸ Since we calculate that the probability of 6-ring formation is 0.34, we can conclude that the extension of a diamond (111) terrace by C_2H is a relaxation process that cannot be observed within less than 1.0 ps (as simulated by Perry et al.¹⁸) or, as in our case, within 2.0 ps, using an MD simulation code. This demonstrates that the inclusion of longer time scale events is necessary when simulating the growth of crystalline structures.

At the diamond (111) step edges, defect formation occurs by the formation of carbon 5-rings (see third column), i.e., by one

bridging adatom between the upper- and lower-lying terraces. No carbon 7-rings are observed, as in the case of the diamond (100) step edges.

The results for the species important for UNCD growth (Tables 1 and 2) show that the behavior of the C_xH_y species is highly dependent on the structure of the step edge: In contrast to the diamond (100) step edge, where C is the most probable species to form carbon 6-rings, this species has the highest probability to form carbon 5-rings (i.e., defects) at the diamond (111) step edge. Furthermore, C_3H_2 contributes to the extension of the diamond structure in the case of the diamond (111) step edge, as distinct from the diamond (100) step edge, where C_3H_2 forms defects with a very high probability.

Migration of hydrocarbon species down the step edge delimiting the diamond (111) terrace is, as in the case of

diamond (100) step edges, not very probable: This mechanism is observed for C_2H , C_3 , and C with a probability of 0.26, 0.06, and 0.04, respectively. Migration of species down a step edge is thus a minor process during UNCD growth.

C_xH_y Species Important for NCD Growth. The results for the species important during NCD growth when stuck to step edges of the diamond (100) and (111) terraces can be found in Tables 3 and 4, respectively. For the step edge at the diamond (100) terrace (see Table 3), CH_2 has the highest probability (0.86) to pursue the diamond crystal structure. Note that it is again a C_1H_y species that has the highest probability to contribute to the extension of the diamond (100) terrace, as in the case of UNCD growth. Besides CH_2 , C_2H_2 is the only species that is able to form new carbon 6-rings at the diamond (100) step edge (with a probability of 0.46). At the diamond (111) terrace, however, it is C_3H_2 that has the highest probability to pursue the diamond structure (see Table 4). Similar to the species important for UNCD growth, the probabilities for the formation of carbon 6-rings are significantly smaller for the diamond (111) step edges (see Table 4) than those at the diamond (100) terrace (see Table 3): C_3H_2 and CH_2 , the species that are the most probable to extend the diamond (111) and (100) terrace, respectively, have 6-ring formation probabilities of 0.34 and 0.86, respectively. In addition, C_2H_2 , which is able to pursue both the diamond (100) and (111) terrace, is less important for the extension of the diamond (111) terrace than for the diamond (100) terrace; the probabilities to form carbon 6-rings at the step edges have values of 0.14 and 0.46, respectively. As already mentioned above, Perry et al. have simulated impacts of C_xH_y species on diamond (111) type B step edges.¹⁸ Of 1000 simulated MD collisions, they found that 38 impacts of C_2H_2 resulted in chemisorption; 28 of these 38 (74%) chemisorbed C_2H_2 subsequently desorbed, and 10 remain stuck within the simulation time.¹⁸ Of those stuck C_2H_2 clusters, 9 C_2H_2 molecules (i.e., 24% of the 38 initial chemisorptions) bridge the step edge, resulting in a new carbon 6-ring. Only one (2% of the 38 initial chemisorptions) of the stuck C_2H_2 clusters remains bonded by only one C–C bond to the step edge. Note that all mechanisms described by Perry et al. (formation of a carbon 6-ring, desorption off the step edge, and remaining stuck by one C–C bond to the step edge) are reproduced by our simulations, as shown in Table 4. The probabilities of the resulting configurations we calculated, however, differ from those that were calculated by Perry et al.¹⁸ This might be due to the fact that the simulation conditions differ; that is, we apply lower system temperature (800 and 1100 K vs 1250 K).

The formation of a carbon 6-ring by C_2H_2 at the diamond (111) step edge is also predicted by Larsson by means of DFT calculations;¹¹ indeed, the configuration containing the carbon 6-ring is the configuration with the greatest energy decrease with respect to the starting configuration (-5.15 eV; see Tables 2 and 4).

The formation of defects by the species important for NCD growth is only seen for C_3H_2 (when adsorbed to a diamond (100) step edge; see Table 3) and for CH_2 (when adsorbed to a diamond (111) step edge; see Table 4). The probability of defect formation in the case of C_3H_2 at the diamond (100) step edge at a temperature of 1100 K (0.96; see Table 3) is comparable to the probability at 800 K (0.98; see Table 1). The probability of defect formation by a C_1H_y species at the diamond (111) step edge is however much lower for the hydrogen richer species important for NCD growth;

that is, compare the 5-ring formation probabilities of CH_2 (0.02; see Table 4) and C , which is important for the growth of UNCD (0.94; see Table 2). Indeed, as more hydrogen atoms are bonded to a carbon atom, the free electrons of that carbon adatom are more shielded from the dangling bond at the surface, which lowers the reactivity.²⁶

For CH_2 at the diamond (111) step edge, Perry et al. do not report the formation of a carbon 5-ring,¹⁸ whereas Larsson predicts the formation of that second C–C bond by means of DFT calculations.¹¹ Indeed, according to the results presented in Table 4, the second C–C bond formation (defect formation) results in the configuration with the lowest energy. Therefore, it must be an infrequent event that is not seen when applying MD but only when considering the longer time scale evolution of the system.

Migration of C_xH_y species from the upper- to the lower-lying terrace is seen for only one case: CH_2 at the diamond (100) step edge. Richley et al. have described this migration of CH_2 by means of hybrid quantum mechanical/molecular mechanics calculations.²⁴ They have calculated the energy of the configuration containing the carbon 6-ring (which is considered to be the intermediate of the migration from the upper- to lower-lying terrace) and the energy of the resulting configuration, i.e., CH_2 at the lower-lying terrace. The relative order of the energetics corresponds remarkably well to our calculations: With respect to the initial configuration, i.e., CH_2 adsorbed at the step edge, the energy decrease due to the carbon 6-ring formation is calculated to be -3.76 eV²⁴ and -2.49 eV (present investigation; see Table 3); the energy decrease when fully migrated to the lower-lying terrace is calculated to equal -1.03 eV²⁴ and -0.43 eV (present investigation; see Table 3). As pointed out by other authors,¹¹ the quantitative predictions made using the Brenner potential must be interpreted with caution; nevertheless, qualitative agreement between the energetic order of configurations predicted by DFT and the Brenner potential was reported as well.¹¹

Similar to the species important for UNCD growth, the probability for migration of CH_2 is rather low (0.06; see Table 3), which allows us to state that migration down a step edge is in general a minor process during CVD diamond growth.

Implications for the Growth Regimes of UNCD and NCD.

In Tables 5 and 6, the species that affect the growth of terraces the most distinctly through either extension or defect formation at step edges are summarized. Besides their probabilities of 6-ring and defect formation, the concentrations of the species close to the surface are presented, i.e., their concentrations at 1 mm from the surface as found in ref 5. Since the temperature gradient is high close to the surface, the concentrations reported in ref 5 and the concentrations at the surface can be expected to differ from each other. In ref 50, the concentrations at 0.5 mm are presented, which should approach the concentrations at the surface to a better extent. However, as the concentrations of C_3H_y and C_3H_y species are only reported at 1 mm distance, and in order to maximize the comparability of the C_xH_y species, the values from ref 5 are presented in Tables 5 and 6. Note, however, that the order of magnitude of the concentrations is constant for the two distances from the surface for all C_1H_y and C_2H_y species, except for C_2H_2 in the case of the NCD growth condition: C_2H_y has a concentration of 2.96×10^{16} cm⁻³ at 0.5 mm, i.e., a concentration that is 100 times higher than that at a distance of 1 mm.

Table 5. Summarizing Table with the Species Important for UNCD Growth That Have the Highest Probabilities of 6-Ring Formation ($P_{6\text{-ring}}$) and Defect Formation (P_{defect})^a

UNCD Species That Contribute to the Step-Flow Mechanism			
terrace	species	$P_{6\text{-ring}}$	conc (cm^{-3})
(100)	C	0.96	2.12×10^{12}
	C ₂ H	0.74	9.15×10^{12}
(111)	C ₂ H	0.34	9.15×10^{12}
	C ₃ H ₂	0.30	3.63×10^{13}
UNCD Species That Form Defects			
terrace	species	P_{defect}	conc (cm^{-3})
(100)	C ₃ H ₂	0.96	3.63×10^{13}
	C ₃	0.70	1.80×10^{14}
(111)	C	0.94	2.12×10^{12}
	C ₃	0.88	1.80×10^{14}

^aTheir concentrations in the gas phase near the growing diamond surface, as calculated in ref 5, are given as well.

Table 6. Summarizing Table with the Species Important for NCD Growth That Have the Highest Probabilities of 6-Ring Formation ($P_{6\text{-ring}}$) and Defect Formation (P_{defect})^a

NCD Species That Contribute to the Step-Flow Mechanism			
terrace	species	$P_{6\text{-ring}}$	conc (cm^{-3})
(100)	CH ₂	0.86	1.34×10^{13} (CH ₃)
	C ₂ H ₂	0.46	2.26×10^{14}
(111)	C ₃ H ₂	0.34	2.32×10^{12}
	C ₂ H ₂	0.14	2.62×10^{14}
NCD Species That Form Defects			
terrace	species	P_{defect}	conc (cm^{-3})
(100)	C ₃ H ₂	0.98	2.32×10^{12}
(111)	CH ₂	0.02	1.34×10^{13} (CH ₃)

^aTheir concentrations in the gas phase near the growing diamond surface, as calculated in ref 5, are given as well.

The C_xH_y species which are important for UNCD growth and very probable to cause a defect at a diamond step edge (i.e., C₃H₂ and C₃; see Table 5) have high concentrations: C₃ has a probability of ≥ 0.70 to form a defect at the step edges of both diamond (100) and (111), and it has a concentration of $1.80 \times 10^{14} \text{ cm}^{-3}$ close to the surface of the growing UNCD film.⁵ The same is true for C₃H₂ at the diamond (100) step edge; the probability of defect formation equals 0.96, and its concentration is rather high ($3.63 \times 10^{13} \text{ cm}^{-3}$). On the other hand, C and C₂H, which contribute to the step-flow mechanism at a growing diamond (100) terrace through the formation of 6-rings with a probability of > 0.7 , however, have lower concentrations close to the growing film ($\sim 10^{12} \text{ cm}^{-3}$; see Table 5). For diamond (111) terraces, only one of the species that contribute the most to the extension at the step edges, C₃H₂, has a moderate concentration ($3.63 \times 10^{13} \text{ cm}^{-3}$). Nevertheless, its probability of 6-ring formation is low (0.30; see Table 5).

When examining the resulting structures of the species important for NCD growth (Tables 3 and 4), it can be seen that there is only one case for which defect formation is observed with a high probability: C₃H₂ at the diamond (100) step edge (see Table 6). Note that the concentration of C₃H₂ is rather low ($2.32 \times 10^{12} \text{ cm}^{-3}$) compared to those of C₂H₂ ($2.62 \times 10^{14} \text{ cm}^{-3}$ at 1 mm above the surface, or even $2.96 \times 10^{16} \text{ cm}^{-3}$ at 0.5 mm above the surface)^{5,50} and CH₃ ($1.34 \times 10^{13} \text{ cm}^{-3}$),⁵ which both contribute to the extension of the diamond structure when adsorbed to the diamond (100) step edges (see Table 6).

Furthermore, for C₂H₂, which is the C_xH_y species with the highest concentration above the growing UNCD film, carbon 6-rings are not the dominant resulting structure when adsorbed to the step edges: C₂H₂ has a concentration of $1.68 \times 10^{15} \text{ cm}^{-3}$ but forms carbon 6-rings at the diamond (100) and (111) step edges with probabilities of only 0.32 and 0.14, respectively (see Tables 1 and 2). During the growth of NCD, the species with the highest concentration above the surface is also C₂H₂ ($2.62 \times 10^{14} \text{ cm}^{-3}$ at 1 mm above the surface, or even $2.96 \times 10^{16} \text{ cm}^{-3}$ at 0.5 mm above the surface);^{5,50} the contribution of C₂H₂ to the step-flow mechanism at the (100) step edge increases to 0.46 (see Tables 3 and 6). However, the probability of 6-ring formation remains constant (0.14) for the diamond (111) step edge (see Tables 4 and 6).

In summary, the different morphologies of UNCD and NCD films can be related to the ability of their growth species to contribute to the step-flow growth mechanism. Indeed, near the growing diamond surface, the concentrations of the UNCD growth species that could extend diamond terraces through the step-flow growth mechanism are relatively low. Additionally, a number of UNCD growth species that cause defect formation with a high probability have a relatively high concentration above the growing UNCD film. The species that are present above the growing UNCD film will thus confine diamond growth through the extension of step edges. In that manner, it can be expected that the step-flow growth mechanism is of no great importance for UNCD growth; in the limit, it will be absent during UNCD growth. Note, however, that the absence of the step-flow mechanism during UNCD growth would not imply that no diamond growth occurs at all; as was shown in ref 30, the applied plasma for UNCD growth contains hydrocarbon species that enable the propagation of the diamond structure at flat diamond surfaces. The contribution of the step-flow mechanism could be quantified by implementing it into more macroscopic growth models, e.g. the kinetic MC model by May and Mankelevich.¹⁴ For the growth species of NCD, the opposite is true: The species that enhance the extension of diamond terraces, i.e., that contribute to the step-flow mechanism, have high concentrations. Moreover, the species that form defects with a high probability at the step edges (i.e., C₃H₂) have a relatively low concentration above the surface of the growing film. In that manner, the species present in the plasma that is applied for NCD growth promote the formation of well-faceted diamond crystals.

As can be concluded from Tables 5 and 6, the C₁H_y species are not the only species that contribute to film growth. Although the configuration of species stuck to step edges during UNCD growth turned out to be doubtful, for UNCD, C₃H₂ and C₃ may be of great importance through defect formation at step edge resembling surface shapes. For NCD, C₂H₂, which has a high concentration above the growing surface, is quite probable to play an important role in the step-flow mechanism, together with CH₂. Taking the recent doubts about the importance of the β -scission reaction during (U)NCD growth into account,¹⁴ it can be stated that the growth model of UNCD and NCD should not be restricted to C₁H_y species. Therefore, we encourage the investigation of reaction pathways of C_xH_y with $x \geq 2$ when stuck to diamond step edges at a higher level of theory.

As discussed above, the growth of diamond through the extension of terraces is more probable for diamond (100) terraces than for diamond (111) terraces. Whereas the probability of

6-ring formation at the diamond (100) step edge is > 0.8 for the most reactive species, all 6-ring formation probabilities at the diamond (111) step edge are < 0.4 . This theoretical observation covers the experimentally known fact that the thicker a growing CVD diamond film becomes, the greater is the relative amount of diamond (100) facets.⁵¹ At maximum, the film surface is completely covered with (100) facets.⁵¹

Conclusions

In the present paper, we investigated the behavior of hydrocarbon species at step edges of diamond terraces by means of a combined MD-MMC approach. The MD part of the model accounts for the simulation of impacting hydrocarbon species onto the diamond structure, and the MMC part simulates the slower relaxation events.

Two types of step edges were considered: The “S_B” step edge delimiting a diamond (100) terrace, and the “type B” step edge at the diamond (111) terrace. Only biradical sites at the step edges were considered; that is, the behavior of the hydrocarbon species when stuck to the vertical plane of the step edge with one dangling bond present at the lower-lying terrace. The investigated species are selected based on their concentrations close to the surface in combination with their sticking coefficients.

For the species important for UNCD growth, it is shown that all species are capable of pursuing the upper-lying terrace (except for C at the diamond (111) step edge). For the diamond (100) terrace, C and C₂H are the species that are the most probable (probability > 0.7) to extend the diamond structure. At the diamond (111) step edge, C₂H and C₃H₂ have the highest probability to pursue the terrace (0.34 and 0.30, respectively). Of the species that are the most important for NCD growth, CH₂ and C₂H₂ are capable of contributing to the extension of the diamond (100) terrace. For the diamond (111) terrace, those species are C₃H₂ and C₂H₂. As for the UNCD growth conditions, the probabilities for the extension of the diamond (100) terrace are much higher than those for the diamond (111) terrace. This theoretical prediction is in full agreement with the experimental observation that diamond (100) facets are more favored than diamond (111) facets during the growth of CVD diamond.

The main conclusion of this investigation is that the different growth regimes of UNCD and NCD can be related to the gas phase concentrations of C_xH_y species in a new fashion: we attempt to explain the formation of ballas-like diamond films (UNCD) by the suppression of the step-flow growth mechanism. During CVD diamond growth, this mechanism is believed to cause the growth of well-faceted CVD diamond films such as NCD. The species that are important for the growth of UNCD have high probabilities to form defects at the step edges. During UNCD growth, those species are present in high concentrations above the growing film. The gas phase species above the growing UNCD film will thus restrict the extension of diamond terraces at the step edges; that is, the step-flow growth mechanism will not play a major role in the growth of UNCD or will even not be valid for the growth of UNCD. For NCD, the opposite is true: The species that enhance the extension of diamond terraces have high concentrations, whereas the species that preferentially form defects are present in lower concentrations above the growing film; the step-flow growth mechanism will thus play an important role during NCD growth, resulting in the typical well-faceted diamond crystals.

Of the species important for UNCD growth, the C₃H_y species are shown to be very reactive. For NCD, C₂H₂, besides CH₂, is predicted to be important for the extension of diamond terraces. Therefore, the growth model of UNCD and NCD should be extended by C_xH_y species with $x \geq 2$, on condition that the behavior of these species is investigated at a higher level of theory.

Acknowledgment. M.E. is indebted to the Institute for the Promotion of Innovation through Science and Technology in Flanders (IWT-Vlaanderen) for financial support. E.N. acknowledges financial support from the Fund for Scientific Research—Flanders (FWO). This work was financially supported by the IAP-P6/42 project “Quantum Effects in Clusters and Nanowires” and the Fund for Scientific Research—Flanders (FWO). The calculation support of the core facility CALCUA, provided by the University of Antwerp, is gratefully acknowledged.

References

- (1) Gruen, D. M. *Annu. Rev. Mater. Sci.* **1999**, *29*, 211–259.
- (2) Philip, J.; Hess, P.; Feygelson, T.; Butler, J. E.; Chattopadhyay, S.; Chen, K. H.; Chen, L. C. *J. Appl. Phys.* **2003**, *93*, 2164–2171.
- (3) Wang, Z. L.; Li, J. J.; Sun, Z. H.; Li, Y. L.; Luo, Q.; Gu, C. Z.; Cui, Z. *J. Appl. Phys. Lett.* **2007**, *90*, 133118.
- (4) Williams, O. A.; Daenen, M.; D’Haen, J.; Haenen, K.; Maes, J.; Moshchalkov, V. V.; Nesládek, M.; Gruen, D. M. *Diamond Relat. Mater.* **2006**, *15*, 654–658.
- (5) May, P. W.; Harvey, J. N.; Smith, J. A.; Mankelevich, Y. A. *J. Appl. Phys.* **2006**, *99*, 104907.
- (6) Donnelly, C. M.; McCollough, R. W.; Geddes, J. *Diamond Relat. Mater.* **1997**, *6*, 787–790.
- (7) Zapol, P.; Sternberg, M.; Curtiss, L. A.; Frauenheim, T.; Gruen, D. M. *Phys. Rev. B* **2002**, *65*, 45403.
- (8) Yang, T.-S.; Lai, J.-Y.; Cheng, C.-L.; Wong, M.-S. *Diamond Relat. Mater.* **2001**, *10*, 2161–2166.
- (9) May, P. W.; Ludlow, W. J.; Hannaway, M.; Heard, P. J.; Smith, J. A.; Rosser, K. N. *Chem. Phys. Lett.* **2007**, *446*, 103–108.
- (10) Angus, J. C.; Will, H. A.; Stanko, W. S. *J. Appl. Phys.* **1968**, *39*, 2915.
- (11) Larsson, K. *Phys. Rev. B* **1997**, *56*, 15452–15458.
- (12) van Enckevort, W. J. P.; Janssen, G.; Vollenberg, W.; Schermer, J. J.; Giling, L. J.; Seal, M. *Diamond Relat. Mater.* **1993**, *2*, 997–1003.
- (13) Netto, A.; Frenklach, M. *Diamond Relat. Mater.* **2005**, *14*, 1630–1646.
- (14) May, P. W.; Allan, N. L.; Ashfold, M. N. R.; Richley, J. C.; Mankelevich, Y. A. *J. Phys.: Condens. Matter* **2009**, *21*, 364203.
- (15) Frenklach, M.; Skokov, S. *J. Phys. Chem. B* **1997**, *101*, 3025–3036.
- (16) Larsson, K.; Carlsson, J.-O. *Phys. Rev. B* **1999**, *59*, 8315–8322.
- (17) Battaile, C. C.; Srolovitz, D. J.; Oleinik, I. I.; Pettifor, D. G.; Sutton, A. P.; Harris, S. J.; Butler, J. E. *J. Chem. Phys.* **1999**, *111*, 4291–4299.
- (18) Perry, M. D.; Raff, L. M. *J. Phys. Chem.* **1994**, *98*, 4375–4381.
- (19) Larsson, K.; Carlsson, J.-O. *Phys. Status Solidi A* **2001**, *186*, 319–330.
- (20) Alfonso, D. R.; Yang, S. H.; Drabold, D. A. *Phys. Rev. B* **1994**, *50*, 15369–15380.
- (21) Skokov, S.; Weiner, B.; Frenklach, M.; Frauenheim, T.; Sternberg, M. *Phys. Rev. B* **1995**, *52*, 5426–5432.
- (22) Frenklach, M.; Skokov, S.; Weiner, B. *Nature* **1994**, *372*, 535–537.
- (23) Cheesman, A.; Harvey, J. N.; Ashfold, N. R. *J. Phys. Chem. A* **2008**, *112*, 11436–11448.
- (24) Richley, J. C.; Harvey, J. N.; Ashfold, M. N. R. *Mater. Res. Soc. Symp. Proc.* **2010**, *1203*, 1203-J17-32.
- (25) Ma, J.; Richley, J. C.; Ashfold, M. N. R.; Mankelevich, Y. A. *J. Appl. Phys.* **2008**, *104*, 103305.
- (26) Eckert, M.; Neyts, E.; Bogaerts, A. *Chem. Vap. Deposition* **2008**, *14*, 213–223.
- (27) Dyson, A. J.; Smith, P. V. *Surf. Sci.* **1994**, *316*, 309–316.
- (28) Doll, J. D.; Voter, A. F. *Annu. Rev. Phys. Chem.* **1987**, *38*, 413–431.
- (29) Eckert, M.; Neyts, E.; Bogaerts, A. *CrystEngComm* **2009**, *11*, 1597–1608.

- (30) Eckert, M.; Neyts, E.; Bogaerts, A. *Cryst. Growth Des.* **2010**, *10*, 3005–3021.
- (31) Metropolis, N.; Rosenbluth, A. W.; Rosenbluth, M. N.; Teller, A. H.; Teller, E. *J. Chem. Phys.* **1953**, *21*, 1087–1092.
- (32) DeVita, J. P.; Sander, L. M.; Smereka, P. *Phys. Rev. B* **2005**, *72*, 205421.
- (33) Metiu, H.; Lu, Y.-T.; Zhang, Z. *Science* **1992**, *255*, 1088–1092.
- (34) Taguchi, M.; Hamaguchi, S. *Thin Solid Films* **2007**, *515*, 4879–4882.
- (35) Tsuno, T.; Tomikawa, T.; Shikata, S.-i. *Appl. Phys. Lett.* **1994**, *64*, 572–574.
- (36) Kreutz, T. J.; Clausing, R. E.; Heatherly, L., Jr.; Warmack, R. J.; Thundat, T.; Feigerle, C. S.; Wandelt, K. *Phys. Rev. B* **1995**, *51*, 14554–14558.
- (37) Kawarada, H.; Sasaki, H.; Sato, A. *Phys. Rev. B* **1995**, *52*, 11351–11358.
- (38) Busmann, H.-G.; Zimmermann-Edling, W.; Sprang, H.; Güntherodt, H.-J.; Hertel, I. V. *Diamond Relat. Mater.* **1992**, *1*, 979–988.
- (39) Chadi, D. J. *Phys. Rev. Lett.* **1987**, *59*, 1691–1987.
- (40) Skokov, S.; Weiner, B.; Frenklach, M. *J. Phys. Chem.* **1994**, *98*, 7073–7082.
- (41) Frenklach, M. *Phys. Rev. B* **1992**, *5*, 9455–9458.
- (42) Butler, J. E.; Mankelevich, Y. A.; Cheesman, A.; Ma, J.; Ashfold, M. N. R. *J. Phys.: Condens. Matter* **2009**, *21*, 364201.
- (43) Frenkel, D.; Smit, B. *Understanding Molecular Simulation*, 1st ed.; Academic Press: San Diego, 1996.
- (44) Brenner, D. W. *Phys. Rev. B* **1990**, *42*, 9458–9471.
- (45) Träskelin, P.; Salonen, E.; Nordlund, K.; Krasheninnikov, A. V.; Keinonen, J.; Wu, C. H. *J. Nucl. Mater.* **2003**, *313–316*, 52–55.
- (46) Barkema, G. T.; Mousseau, N. *Phys. Rev. Lett.* **1996**, *77*, 4358–4361.
- (47) Liu, Y. H.; Neyts, E.; Bogaerts, A. *Diamond Relat. Mater.* **2006**, *15*, 1629–1635.
- (48) Henkelman, G.; Jónsson, H. *Phys. Rev. Lett.* **2003**, *90*, 116101.
- (49) Landau, D. P.; Binder, K. A. *Guide to Monte Carlo Simulations in Statistical Physics*, 1st ed.; Cambridge University Press: Cambridge, 2000.
- (50) May, P. W.; Mankelevich, Y. A. *J. Phys. Chem. C* **2008**, *112*, 12432–12441.
- (51) Wild, C.; Koidl, P.; Müller-Sebert, W.; Walcher, H.; Kohl, R.; Herres, N.; Locher, R.; Samlenski, R.; Brenn, R. *Diamond Relat. Mater.* **1993**, *2*, 158–168.